

Article

Experimental Assessment of Mechanical Properties of Corroded Low-Alloy Structural Steel

Yao Chen ^{1,*}, Boshi Ma ¹ and Ruihua Lu ²

¹ School of Civil Engineering and Architecture, Jiangsu University of Science and Technology, Zhenjiang 212100, China; 202210901421@stu.just.edu.cn

² Key Laboratory of Concrete and Prestressed Concrete Structures of Ministry of Education, School of Civil Engineering, Southeast University, Nanjing 211189, China; 101005635@seu.edu.cn

* Correspondence: chenya0727@just.edu.cn

Abstract: This study investigates the mechanical properties of corroded Q355B structural steel subjected to a simulated marine atmosphere and an industrial atmosphere. The micro-morphology of corroded steel in two different environments was analyzed by SEM (scanning electron microscopy). Tension tests were performed to determine the degradation laws of the mechanical properties of corroded steel, including its yield strength, ultimate strength, elastic modulus, ultimate strain and elongation after fracture. The test results indicate that the elongation after fracture of the steel is the most severely deteriorated property after corrosion. The recommended empirical formula for limiting the maximum corrosion rate is established. It is found that when the initial elongation is 30%, the maximum allowable corrosion rate is 19.2%. Based on the achieved results, a simplified time-dependent stress–strain model of Q355B structural steel is established considering the coupling effects of corrosive environments and applied stress, which is also evaluated using relevant research. In addition, axial compression tests were conducted on corroded square stud columns to verify the effectiveness of the established model. It is indicated that the model can be used for fitness-for-purpose analyses in structural integrity assessments.

Keywords: corroded steel; tension tests; mechanical properties; time-dependent stress–strain model; axial compression tests



Citation: Chen, Y.; Ma, B.; Lu, R.

Experimental Assessment of Mechanical Properties of Corroded Low-Alloy Structural Steel. *Buildings* **2024**, *14*, 1457. <https://doi.org/10.3390/buildings14051457>

Academic Editors: Michael Raupach and Sylvia Kessler

Received: 20 April 2024

Revised: 11 May 2024

Accepted: 14 May 2024

Published: 17 May 2024



Copyright: © 2024 by the authors. Licensee MDPI, Basel, Switzerland. This article is an open access article distributed under the terms and conditions of the Creative Commons Attribution (CC BY) license (<https://creativecommons.org/licenses/by/4.0/>).

1. Introduction

Corrosion can lead to structural material degradation, reduce mechanical properties, and facilitate fatigue cracks, brittle fractures and unstable failures, affecting the safety and life of structures. Specifically, the study of the degradation laws of the mechanical properties of corroded steel is the basis for further predicting the reliability and remaining life of steel structures. Currently, extensive research has been carried out on the mechanical properties of corroded mild steel, and certain research results have been recorded.

In the early studies, the remaining capacity of corroded steel established by researchers was mainly based on ‘the minimum cross-section theory’ (maximum corrosion rate). Paik et al. [1] conducted experimental research on the capacity of plates with different levels of pitting corrosion under axial compression. The research results indicate that the ultimate strength of plates with pitting damage is determined by the minimum cross-sectional area (maximum corrosion rate) at the location of pitting corrosion and establish formulas for the strength reduction factor based on the minimum cross-sectional area of the plates. Yamamoto et al. [2] simulated natural corrosion through mechanical pitting and obtained tensile specimens with different pit depths and patterns. Their study showed that the strength decreases gradually and the total elongation decreases drastically with the increase of the thickness loss due to pitting corrosion. It also proved that the decrease in tensile strength caused by pitting corrosion was greater than that caused by general corrosion under the same conditions. Later, Ahmmad et al. [3] adopted a mechanical

pitting method to produce general corroded specimens and randomly pitted them using different pit sizes, quantities and densities for tensile testing. Their research results verified that the capacity reduction factor for the corroded specimen is consistent with the Paik's model [1], and the reduction factor for the percentage elongation after fracture is related to the maximum surface roughness of the specimens. Appuhamy et al. [4] conducted material tensile tests on actual Q235 corroded steel beams in a marine environment. They found that the mechanical properties of the specimens, including the elongation, yield strength and ultimate strength, showed a decreasing trend with an increasing corrosion rate. A formula was proposed for the residual strength reduction factor using the effective thickness as a factor that is related to the maximum corrosion depth.

In recent years, researchers have conducted some relevant experimental studies on the mechanical properties of corroded steel based on the 'average corrosion rate'. Tong et al. [5] conducted salt spray tests of Q235B steel with and without coating, respectively, to study their yielding strength, tensile strength and elongation. However, the effect of corrosive environments on the corrosion morphology of steel was not considered. Zheng et al. [6,7] studied the mechanical properties of Q235B steel subjected to a simulated acidic atmospheric environment and an offshore atmospheric environment. But a unified mechanical property degradation model has not been established, and the micro-morphology of steel subjected to different corrosive environments has not been analyzed in detail. Garbatov et al. [8–10] obtained natural corroded and marine-immersed corroded Q235B steel plates to study the influence of sandblasting and the sandpaper cleaning method on their mechanical properties and proposed a bilinear stress–strain model of the corroded steel plates. Other different accelerated corrosion methods, such as mechanical drilling [1–3,11], electrochemical corrosion [12] and finite analyses [4,11,13–15], were adopted to obtain pitting corroded steel. Obviously, mechanical drilling and finite element simulation methods simulate pitting corrosion only from the perspective of geometric dimensions, neglecting the impact of chemical composition changes on the mechanical properties of steel.

Currently, researchers have gradually begun to investigate the mechanical properties of corroded high-strength low-alloy steels [16,17]. Zhao et al. [16] proposed a bilinear constitutive model and Rasmussen's model to determine the stress–strain relationship of corroded Q345 and Q420 structural steels but did not study the micro-morphology of the corroded steels. Jia et al. [17] carried out seven groups of copper accelerated acetate spray corrosion tests for Q690E-grade high-strength low-alloy steel plates to investigate their mechanical properties. It is revealed that high-strength steels are more sensitive to corrosion damage than mild steel. However, the applicability of these research results to Q355 low-alloy structural steel needs to be further studied.

In summary, a lot of research has been conducted on the degradation laws of the mechanical properties of steel after corrosion and different prediction models have been established. Various parameters were adopted as representative values of the remaining cross-sectional thickness (i.e., minimum thickness, equivalent thickness). There is controversy among scholars regarding the selection of the representative value for the remaining cross-section or thickness, and a unified opinion has not been formed. The average corrosion pitting depth is an effective factor to evaluate the effect of corrosion depth on the mechanical properties of steels [18]. Although the remaining capacity model of corroded steel established based on the 'maximum cross-sectional corrosion rate' as the influencing factor is more accurate than the model established based on the 'average corrosion rate'. However, it has not been widely applied in actual engineering. The main reasons for this are as follows: the remaining capacity prediction formula based on the 'maximum cross-sectional corrosion rate' as the influencing factor is difficult to obtain in practical applications. It increases the difficulty in predicting the degradation of mechanical properties of materials and members in a corrosive environment. Additionally, current corrosion depth models are developed based on the concept of the 'average corrosion', making it difficult to directly establish a relationship with the capacity calculation formula based on the 'maximum cross-sectional corrosion rate'.

Current research on the mechanical properties of corroded steel is mainly focused on mild steel [1–15], and a few studies have been conducted on low-alloy corroded structural steel [16,17]. At the same time, studies of the micro-morphology of corroded steel are insufficient, especially the difference of the micro-morphology of corroded steel under different corrosion environments. In the established degradation models of material mechanical properties, a unified time-dependent stress–strain curve for corroded steel has not yet been established considering the coupling effect of a corrosive environment and external stress, leading to a lack of reference for further accurately evaluating the remaining life of steel structures. Moreover, the current recommended the maximum limiting value for the corrosion rate of steel, which was proposed by Soares [19] to be 20%, is relatively general and requires further detailed analyses.

Based on the aforementioned questions, this study conducted a salt spray test and an alternate immersion test to obtain corroded Q355B structural steel specimens with different corrosion rates. The differences in the micro-morphology of specimens subjected to two different simulated corrosive environments were analyzed. The tensile test was performed, and degradation models for the material mechanical properties of steel as the corrosion rate increases were established. Combined with the requirements for the mechanical properties of steel in specification, the recommended formula for calculating the maximum allowable corrosion rate based on the initial elongation of steel is proposed. A unified time-dependent stress–strain model for corroded steel is developed, and then its effectiveness is verified by the axial compression tests of four corroded stud columns. This stress–strain model can predict the mechanical properties of corroded Q355B structural steel, and the aged steel structures were further analyzed.

2. Corroded Test Specimens

2.1. Accelerated Corrosion Test

The test specimens are low-alloy structural steel with a thickness of 4 mm and yield stress of 355 MPa. The location and preparation of the specimens meet the requirements of the code GB /T2975 [20]. The geometric dimensions of the test specimens are designed according to GB /T228.1 [21], as shown in Figure 1.

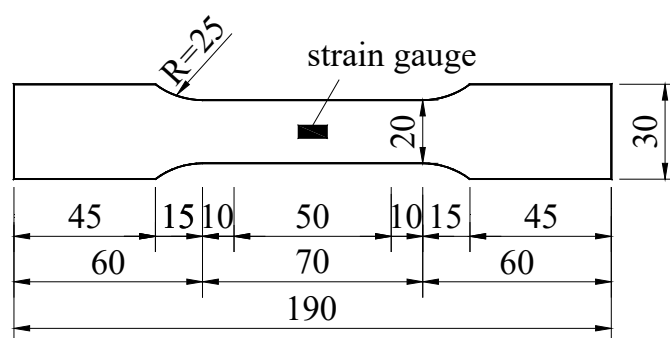


Figure 1. Geometric dimensions of specimen. Unit: mm.

The chemical components of low-alloy structural steel used for specimens are presented in Table 1 as weight percentages, which meet the requirements of the code GB/T 1591 [22].

Table 1. Chemical composition of low-alloy structural steel.

Elements	C	Si	Mn	P	S	V	Cr	Ni	Cu	Mo	Als
Concentration, wt (%)	0.158	0.249	1.23	0.0132	0.0051	0.0019	0.0219	0.0061	0.0052	<0.0020	0.0320

The low-alloy structural steel specimens subjected to a marine atmospheric environment and an industrial atmospheric environment were simulated by two accelerated

corrosion methods, which are detailed in Table 2 [23–29]. The total number of test specimens is 27, including 3 non-corroded specimens and 24 corroded specimens.

Table 2. Accelerated corrosion test conditions.

Corrosion Method	Simulated Environment	Corrosive Solution	Test Conditions	Corrosion Time (h)	Num.
Non-corroded	-	-	-	-	3
Salt spray test	Marine atmosphere	3.5%NaCl + 0.001 mol/L NaHSO ₃	Temperature: 35 °C ± 2 °C; Humidity: >95% RH; pH: 6.5~7.2; Spray air pressure: 120 MPa ± 5 MPa; Cycle period: 12 h (Spray: 6 h and pause: 6 h)	600, 1200, 1800, 2400, 3000, 3600, 4200	14
Alternate immersion test	Industrial atmosphere	0.01 mol/L NaHSO ₃ + 0.001 mol/L NaCl	Temperature: 45 °C ± 2 °C; Humidity: 70 ± 5% RH; pH: 4.4~4.8; Cycle period: 120 min (waterflooding: 18 min, immersion: 20 min, drainage: 18 min, air drying: 8 min, drying: 50 min, and cooling: 6 min)	120, 240, 480, 720, 960	10
				Total	27

The marine atmospheric environment was simulated using the salt spray test, including seven corrosion cycles of 600 h, 1200 h, 1800 h, 2400 h, 3000 h, 3600 h and 4200 h, respectively [5]. As there are many factors affecting the corrosion of steel, the salt spray test method uses a single NaCl solution as the corrosion medium, and the test data obtained cannot be used as a direct basis for the corrosion resistance of the tested material in all operating environments [23]. The reference [27] proved that the adoption of a 3.5% NaCl + 0.001 mol/L NaHSO₃ corrosion solution had a good level of correlation to simulate a marine atmospheric environment. Therefore, a mixed solution of 3.5% NaCl + 0.001 mol/L NaHSO₃ was selected as the spray medium in this research. According to the literature [28] and the condition of the test equipment, a cycle is continuous spraying for 6 h followed by a 6 h pause in spraying, and the other test conditions follow the specification of GB/T 10125 [23].

The industrial atmospheric environment was simulated by an alternate immersion test, including five corrosion cycles of 120 h, 240 h, 480 h, 720 h and 960 h, respectively [27]. The corrosion solution used to simulate the industrial atmospheric environment is 0.01 mol/L NaHSO₃ + 0.001 mol/L NaCl [25], the temperature is 45 °C ± 2 °C, the pH value is controlled at 4.4~4.8, and other test conditions follow the provisions of GB/T 19746 [26].

2.2. Morphologies of Test Specimens

The morphologies of the test specimens subjected to the salt spray test and alternate immersion test are shown in Figures 2a and 2b, respectively (labels A and B represent two parallel specimens from the same corrosion cycle). It can be observed from Figure 2 that there are some differences in the corrosion morphology of the specimens subjected to the two different simulated corrosive environments. Specifically, the corroded specimens subjected to the salt spray test (the marine atmosphere) were blackish-brown in color, and their surface roughness was high, as shown in Figure 2a. The outer layer of the specimen was hard, while the inner layer was soft. The morphologies of the test specimens subjected to the alternate immersion test (the industrial atmosphere) were orange-red in color. The surface roughness of the specimens in the alternate immersion test was lower than that in the salt spray test. The corrosion products were soft and in layers, with blistering.



Figure 2. Morphologies of corroded specimens. (a) Specimens subjected to salt spray test; (b) specimens subjected to alternate immersion test.

The micro-morphology scanning results of the rust layer of the corroded specimens using SEM is shown in Figure 3. For the specimens subjected to the salt spray test, transverse and longitudinal cracks appeared locally on the specimen surface in the early corrosion cycle (Figure 3a, 600 h). The appearance of cracks opened channels for the penetration of oxygen, increasing the activity of metal ions. Spherical iron oxide products have already formed at this time. In the later corrosion cycle (Figure 3b, 4200 h), the surface corrosion products of the steel increased to a certain thickness and became dense. Surface irregularities, evident pitting and the appearance of central voids were observed. The corrosion products gradually filled the cracks, effectively preventing the penetration of oxygen and corrosive media, resulting in a decrease in the corrosion rate of the steel.

For the specimens subjected to the alternate immersion test, numerous transverse and longitudinal intersecting cracks appeared on the specimen surface at the corrosion time of 120 h, as shown in Figure 3c. The difference between the cracks produced by the salt spray test at 600 h, and those produced by the alternate immersion test is that the cracks under the alternate immersion test are shallower but more numerous, connected with each other and distributed across the entire surface of the specimen. When the corrosion time was 960 h, the specimen surface was covered with a large number of spherical oxidation products, as shown in Figure 3d. Compared with the initial corrosion, the cracks developed

rapidly, and the specimen surface was porous, soft and accompanied by cracks and layers, which was consistent with the observed results.

Compared with the salt spray test specimens, the cracks developed rapidly, and the surface of the specimens were porous, soft and accompanied by delamination, which were consistent with the observed corrosion morphology.

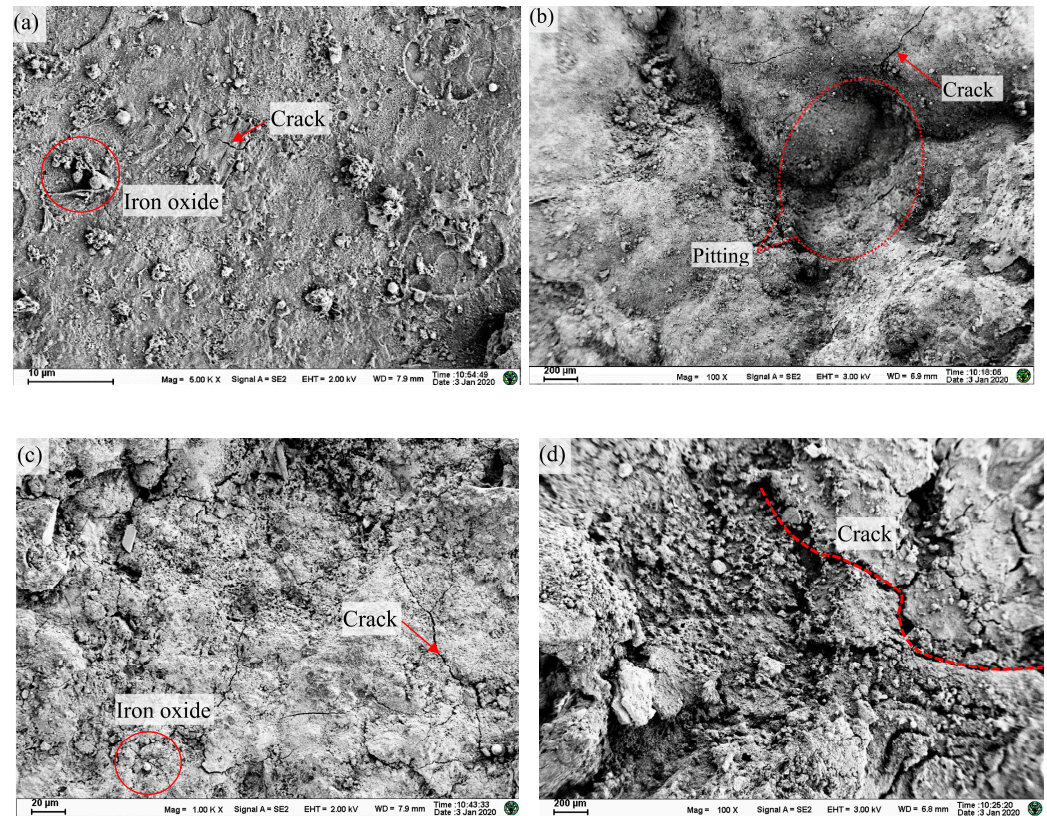


Figure 3. Micro-morphology of corroded specimens. (a) Salt spray test specimen (600 h); (b) salt spray test specimen (4200 h); (c) alternate immersion test specimen (120 h); and (d) alternate immersion test specimen (960 h).

The SEM scanning results can reveal the corrosion degradation laws of steel over time from the microscopic aspect. It is revealed that there are some differences in the micro-morphology of the corroded steel subjected to the simulated marine atmosphere and the industrial atmosphere. The result indicated that the observation is consistent with the results of microscopic scanning by SEM.

2.3. Corrosion Rate of Test Specimens

In order to accurately obtain the corrosion rate of specimens, a rust removal treatment was performed on each specimen before the tensile test according to the code ISO 8407 [30]. After the rust was removed, the specimens were dried and weighed. The average corrosion depths of the specimens under the accelerated corrosion test are obtained by Equation (1), and the results of non-linear fitting curves are shown in Figure 4.

The average corrosion rate of a specimen is calculated by the following formula:

$$c = \frac{m_0 - m_1}{m_0} = \frac{d(t)}{t_0} \quad (1)$$

where c is the average corrosion rate of the specimen; m_0 is the initial mass of the specimen; m_1 is the residual mass of the specimen after corrosion; $d(t)$ is the average corrosion depth of the specimen; and t_0 is the initial thickness of the specimen.

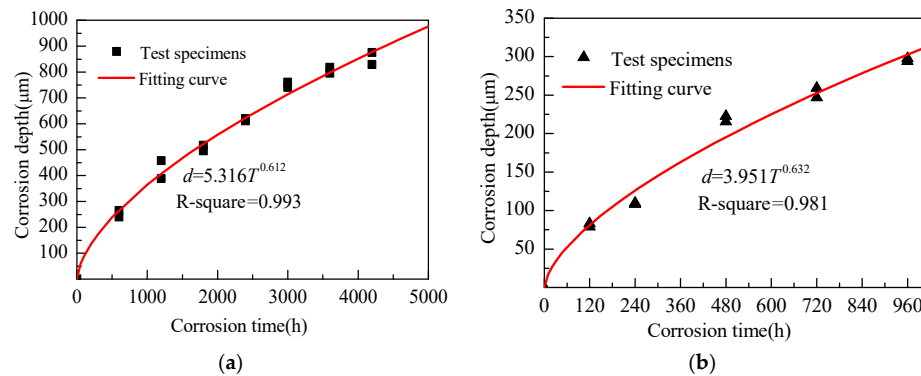


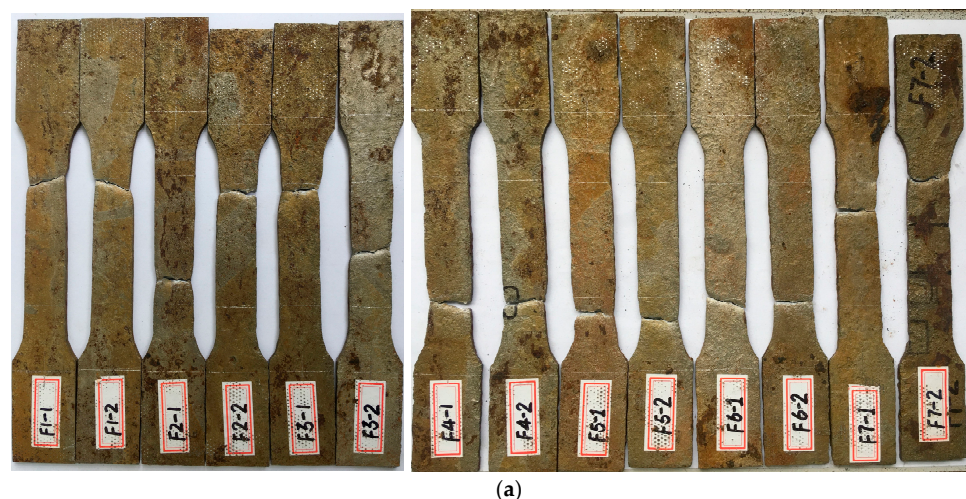
Figure 4. Relationship curves between corrosion depth and time of test specimens. (a) Specimens subjected to salt spray test; (b) specimens subjected to alternate immersion test.

3. Tensile Test

3.1. Tensile Test Process

The tensile test was conducted using a 50 kN electronic universal material test tensile machine (CMT5105) manufactured by SUNS (Shenzhen, China). In order to obtain the percentage elongation after fracture, the gauge length was drawn on both sides of specimens, 25 mm from the centerline on each side. A model SANJ Y50/10 extensometer manufactured by SUNS (Shenzhen, China) was used, with a reference segment of 50 mm and a measuring range of 10 mm. Prior to the test, strain gauges were attached to the central points on both sides of the specimen to calibrate the strain measurement of the extensometer. In the tensile test, the loading rate of the steel before yielding was set at 1 mm/min, and the loading rate gradually increased to 5 mm/min after yielding. The loading rate was increased from 1 mm/min to 5 mm/min using multistage increments.

The failure modes of the specimens with different corrosion rates after fracture are shown in Figure 5. The non-corroded specimens exhibit good ductility, with an obvious necking phenomenon, as shown in Figure 5c. From Figure 5a,b, it can be seen that the stress concentration of the corroded specimens was mainly at the largest pitting, and that of the fractured specimens was at the smallest cross-section. As the corrosion rate increases, the fracture morphology of the specimen transitions from serrated or stepped to slant or flat, and the ductility gradually decreases, leading to brittle failure, which occurs suddenly. Due to the randomness of pitting corrosion after corrosion, the fracture location of the corroded specimen also exhibits randomness. It can be seen that different corrosion environments have a minor impact on the post-fracture morphology of the specimens. The failure morphology of the specimens is mainly related to the corrosion rate.



(a)

Figure 5. Cont.

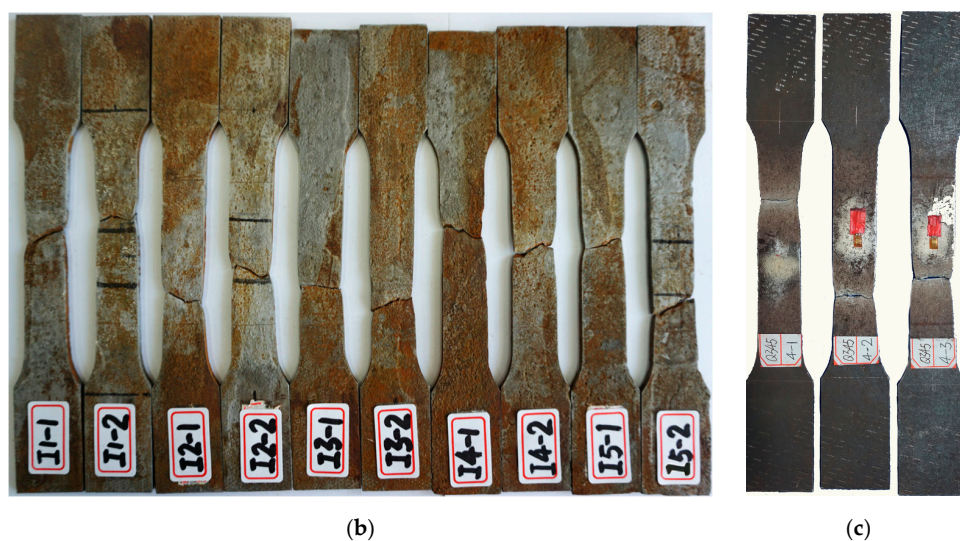


Figure 5. Failure modes of specimens after tensile fracture. (a) Corroded specimens subjected to salt spray test; (b) corroded specimens subjected to alternate immersion test; (c) non-corroded specimens.

3.2. Stress–Strain Curves

The mechanical properties of the steel obtained by the material tensile test are detailed in Table 3. In the table, c is the average corrosion rate. A_r is the remaining average cross-sectional area of the specimen. (For the non-corroded specimens, $A_r = A_0$, measured with a vernier caliper, representing the initial cross-sectional area of the specimen. For the corroded specimens, $A_r = A_0(1 - c)$ is determined by the weight loss method, representing the remaining cross-sectional area of the specimen.) F_c is the ultimate tensile capacity of the specimens (For the non-corroded steel, $F_c = F_0$). σ_{yc} is the yield strength of the specimen. (For the non-corroded specimens, $\sigma_{yc} = \sigma_{y0}$; for the corroded specimens with no obvious yield platform, the residual strain corresponding to a stress of 0.2% is taken as the nominal yield strength.) σ_{uc} is the ultimate strength of the specimen (For the non-corroded specimens, $\sigma_{uc} = \sigma_{u0}$). E_c is the elastic modulus of the specimen. ε_b is the strain corresponding to the ultimate capacity of the specimen. δ is the percentage elongation after fracture of the specimens.

According to the code GB50011 [31], the ratio of the yield strength to the tensile strength of the structural steel should not exceed 0.85. Moreover, the steel should have an obvious yield platform, and the percentage elongation δ should not be less than 20%. From Table 3, it can be seen that as the corrosion rate increases, the yield strength, ultimate strength, elastic modulus and elongation after fracture of the steel all exhibit decreasing trends with the increase in corrosion rate. It is worth noting that the elongation after fracture is the most severely deteriorated property with the increase in the corrosion rate. Starting from a corrosion rate of approximately 11.83% (except for specimen I3-1 at 7.23%), the percentage elongation after fracture cannot meet the requirements of the specification (highlighted in bold in Table 3), indicating that the elongation after fracture of the steel is highly sensitive to corrosion.

The stress–strain curves of the specimens under different corrosion environments and times are shown in Figure 6. It can be seen that the stress–strain curves of the corroded steel exhibit significant changes compared with those of the non-corroded steel, which manifest in the following aspects:

- (1) With the increase in the corrosion rate, the yield strength of the specimen slightly decreases, and the length of the yield platform in the stress–strain curve gradually shortens or even disappears. The yield platform of the corroded specimen begins to gradually disappear at the third corrosion cycle (F3), with a corrosion rate of approximately 13%.

- (2) With the increase in the corrosion rate, the strengthening stage of the stress–strain curve becomes significantly shortened compared to the non-corroded specimens, the ultimate strain value ϵ_b decreases, and the necking stage gradually disappears.
- (3) With the increase in the corrosion rate, the corrosion brittle fracture failure of the specimen becomes more obvious, and the percentage elongation after fracture decreases significantly.
- (4) The corrosive environment mainly affects the corrosion morphology and corrosion rate of steel but has no significant effects on the degradation laws of the mechanical properties of steel.

Table 3. The mechanical properties of specimens.

Specimens	c (%)	A_r (mm ²)	F_c (kN)	σ_{yc} (MPa)	σ_{uc} (MPa)	E_c (GPa)	ϵ_b	$\frac{F_c}{F_0}$	$\frac{\sigma_{yc}}{\sigma_{y0}}$	$\frac{\sigma_{uc}}{\sigma_{u0}}$	δ (%)
4-0-1	0	79.28	40.03	410.1	517.5	200.9	0.169	0.981	0.993	0.997	27.4
4-0-2	0	78.92	40.85	413.6	517.6	200.1	0.151	1.001	1.001	0.997	27.2
4-0-3	0	79.56	41.58	415.7	522.6	201.8	0.162	1.019	1.006	1.006	30.4
F1-1 *	6.13	74.35	39.64	425.3	533.2	197.1	0.137	0.971	1.029	1.027	25.9
F1-2	6.80	73.81	37.18	395.4	503.7	196.7	0.112	0.911	0.957	0.970	24.2
F2-1	10.09	71.21	35.56	391.9	499.4	194.6	0.129	0.871	0.949	0.962	24.7
F2-2	11.83	69.83	34.18	381.9	489.5	193.0	0.141	0.837	0.924	0.943	19.5
F3-1	13.27	68.69	35.15	397.1	511.7	191.5	0.118	0.861	0.961	0.985	19.6
F3-2	12.76	69.09	35.12	396.9	508.3	190.2	0.131	0.860	0.961	0.979	22.2
F4-1	16.23	66.35	33.05	382.6	498.1	189.4	0.087	0.810	0.926	0.959	13.0
F4-2	15.70	66.77	34.60	398.6	518.2	188.9	0.096	0.848	0.965	0.998	19.1
F5-1	19.45	63.80	30.49	375.7	477.9	187.9	0.111	0.747	0.909	0.920	12.0
F5-2	19.19	64.00	32.10	376.6	501.6	187.0	0.091	0.786	0.912	0.966	10.6
F6-1	20.94	62.62	29.43	355.4	470.0	187.9	0.116	0.721	0.860	0.905	12.9
F6-2	20.28	63.14	30.34	376.1	480.5	187.2	0.078	0.743	0.910	0.925	10.8
F7-1	21.29	62.34	30.64	375.4	491.5	186.7	0.085	0.751	0.909	0.947	13.8
F7-2	22.45	61.42	28.33	352.1	461.3	185.0	0.074	0.694	0.852	0.888	9.6
I1-1	2.98	76.84	40.68	401.9	529.3	199.3	0.155	0.996	0.973	1.019	28.0
I1-2	2.84	76.95	41.05	411.2	533.5	199.7	0.153	1.006	0.995	1.027	27.8
I2-1	4.09	75.96	39.64	402.4	521.9	199.1	0.162	0.971	0.974	1.005	25.6
I2-2	4.02	76.02	40.02	396.5	526.4	197.3	0.148	0.980	0.960	1.014	23.0
I3-1	7.29	73.43	38.05	407.2	518.1	194.6	0.111	0.932	0.986	0.998	19.6
I3-2	8.09	72.79	37.58	393.3	516.3	194.8	0.127	0.921	0.952	0.994	23.2
I4-1	8.77	72.25	37.02	389.9	512.4	195.5	0.135	0.907	0.944	0.987	21.6
I4-2	8.96	72.10	36.64	395.9	508.2	195.1	0.131	0.898	0.958	0.979	20.9
I5-1	10.37	70.99	36.00	394.9	507.2	194.6	0.106	0.882	0.956	0.977	22.1
I5-2	10.55	70.84	35.95	398.7	507.5	193.5	0.104	0.881	0.965	0.977	23.1

1. For FX–Z, F represents the specimen subjected to salt spray test; X is the corrosion test cycle (1–7 corresponds to corrosion times of 600 h, 1200 h, 1800 h, 2400 h, 3000 h, 3600 h and 4200 h, respectively); and Z is ‘1’ or ‘2’ indicating two parallel specimens. 2. For IX–Z, I represents the specimen subjected to alternate immersion test; X is the corrosion test cycle (1–5 corresponds to corrosion times of 120 h, 240 h, 480 h, 720 h and 960 h, respectively); and Z is ‘1’ or ‘2’ indicating two parallel specimens. 3. For specimen F1-1 *, the loading rate of 5 mm/min was adopted throughout the tensile test of the specimen, leading to higher yield strength and ultimate strength test results than those of the parallel specimen F1-2. In regards to abnormal deviations in data, these data were excluded from analysis and formula fitting.

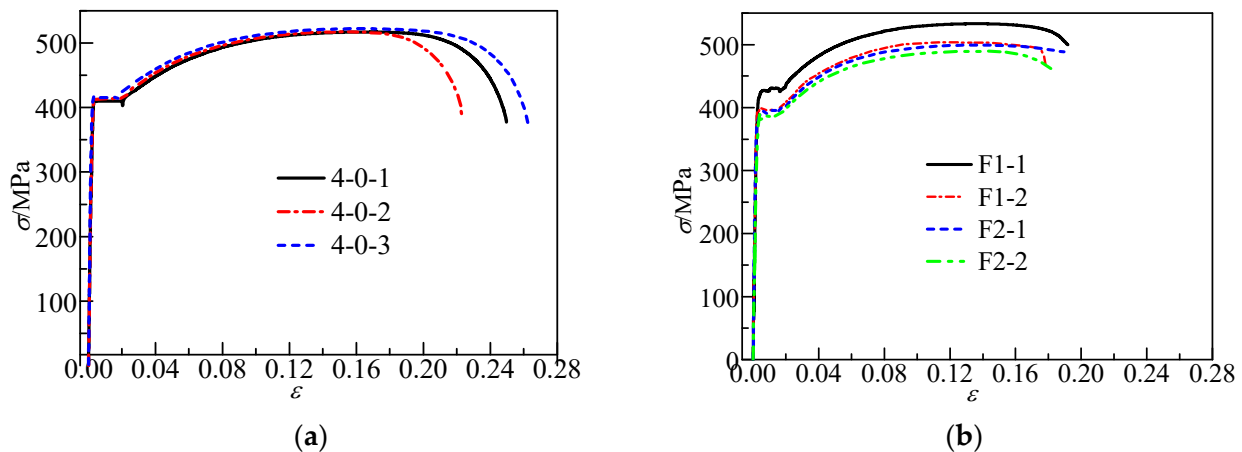


Figure 6. Cont.

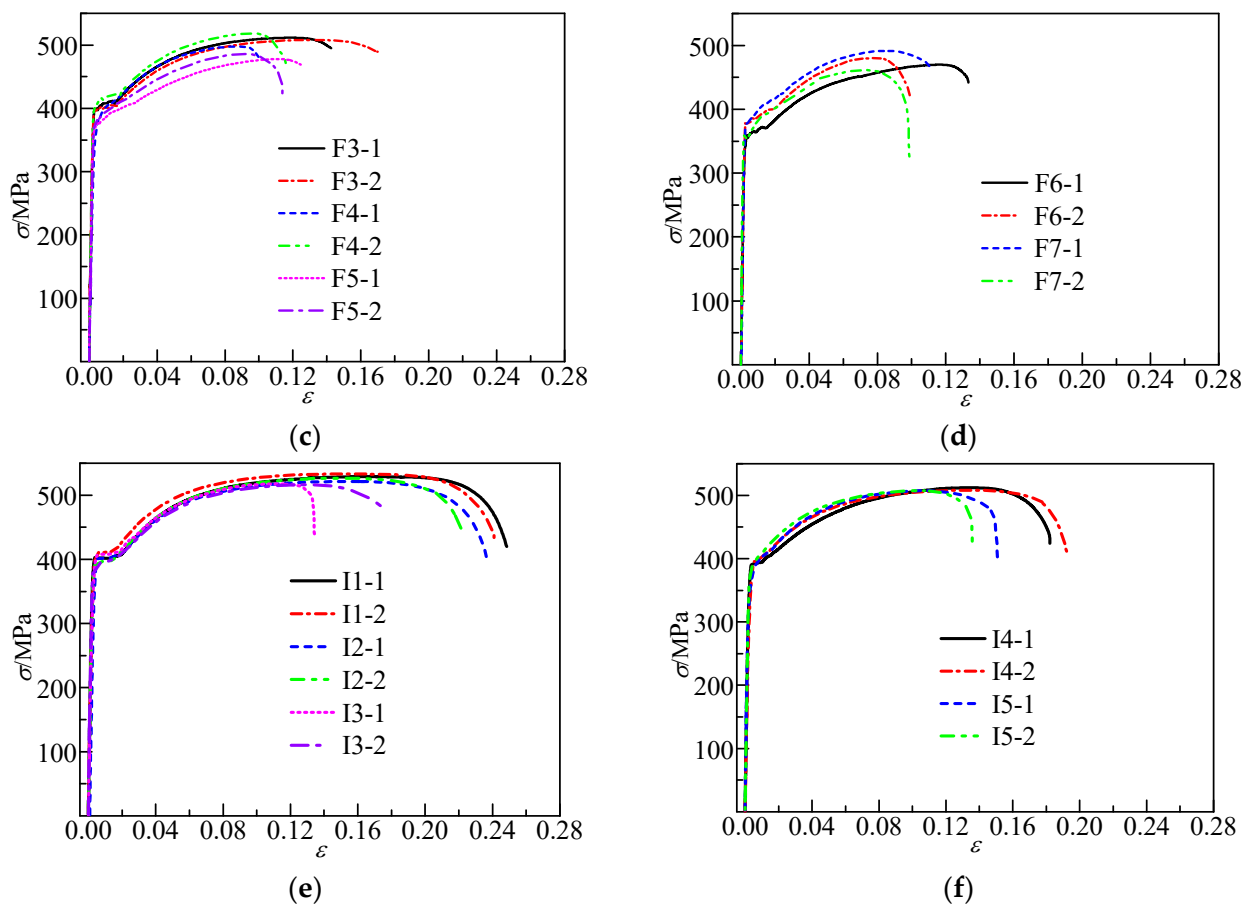


Figure 6. Stress–strain curves of specimens. (a) Non-corroded specimens; (b) salt spray test specimens (600 h and 1200 h); (c) salt spray test specimens (1800 h, 2400 h and 3000 h); (d) salt spray test specimens (3600 h and 4200 h); (e) alternate immersion specimens (120 h, 240 h and 480 h); (f) alternate immersion specimens (720 h and 960 h).

4. Prediction Model for Mechanical Properties of Corroded Steel

The mechanical properties of the corroded steel obtained by material tensile tests include the following: ultimate tensile capacity, yield strength, ultimate strength, elastic modulus, ultimate strain and percentage elongation after fracture. In the following, the degradation laws of the mechanical properties of corroded steel with the increasing corrosion rate are studied in detail.

4.1. Prediction Model for Tensile Ultimate Capacity of Corroded Steel

The reduction factor of the ultimate capacity R_{ut} is defined as the tensile ultimate capacity of the corroded steel divided by the tensile ultimate capacity of the non-corroded steel. The relationship between the ultimate capacity reduction factor R_{ut} and the average corrosion rate c is shown in Figure 7 (The solid dots represent the data of the corroded specimens subjected to the salt spray test, and the hollow dots represent the data of the corroded specimens subjected to the alternate immersion test). Through a non-linear fitting regression, the formula for calculating the ultimate capacity of the corroded steel can be obtained as follows:

$$R_{ut} = F_{tc}/F_0 = (1 - c)^{1.258} \quad (2)$$

where F_{tc} is the tensile ultimate capacity of the corroded steel; F_0 is the tensile ultimate capacity of the non-corroded steel; and c is the average corrosion rate of the steel.

It can be seen from Figure 7 that Equation (2) has a goodness of fit (R-square) of 0.947 for the experimental data, and the residual standard deviation (RMSE) is 0.0206, indicating a good fit between the formula and test results.

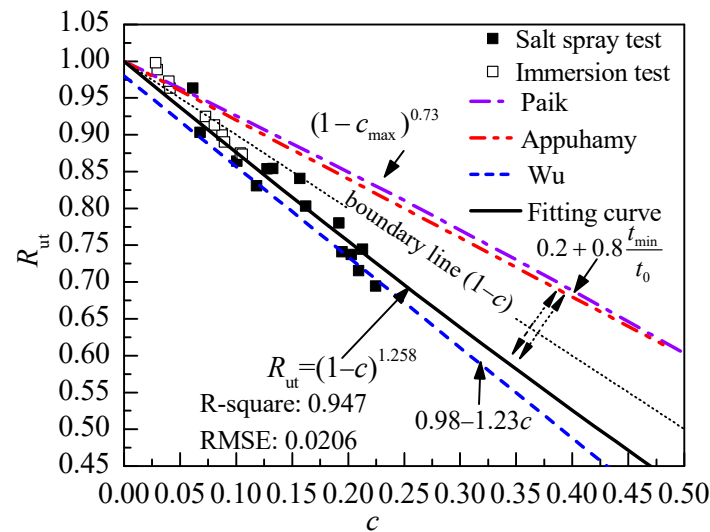


Figure 7. Relationship between the ultimate capacity reduction factor and corrosion rate [1,4,9].

Current research results indicate that the tensile ultimate capacity of the corroded steel is governed by the maximum cross-sectional corrosion rate (the minimum cross-sectional area) of the steel. The commonly used models such as Equation (3), which is proposed by Paik et al. [1], and Equation (4), which is proposed by Appuhamy et al. [4], are as follows:

$$R_{ut} = (1 - c_{max})^{0.73} \quad (3)$$

$$R_{ut} = 0.2 + 0.8 \frac{t_{min}}{t_0} \quad (4)$$

where c_{max} is the maximum corrosion rate of the steel; t_{min} is the minimum thickness of the steel; and t_0 is the initial thickness of the steel.

In recent years, researchers have conducted some relevant experimental studies on calculating the strength of corroded steel based on the 'average corrosion rate'. Xia [11] created elliptical blind holes with different sizes on steel plates to simulate natural pitting corrosion by mechanical drilling methods. Taking the 'average cross-sectional corrosion' as the influencing factor, a formula for calculating the nominal ultimate strength reduction factor of corroded steel was established as follows:

$$R_{ut} = 0.98 - 1.23c \quad (5)$$

where R_{ut} is the nominal ultimate strength reduction factor; and c is the average corrosion rate.

The comparison between Paik's model, Appuhamy's model, Xia's model and the experimental results of this study is shown in Figure 7. It can be observed that there is a significant difference in prediction formulas based on the 'maximum cross-sectional corrosion rate' and 'average cross-sectional corrosion rate' as influencing factors. The reason for the differences is that the randomly formed pitting changed the surface morphology of the steel to some extent (from a smooth and flat surface to a rough and irregular surface). Therefore, the prediction models based on the 'maximum cross-sectional corrosion rate' and 'average cross-sectional corrosion rate' are obtained by modifying the general corroded steel plate degradation model ' $R_{ut} = 1 - c$ ' according to different trajectories, as shown in Figure 7. The main factors affecting these 'trajectories' are the corrosion morphology of the steel, including the maximum pitting diameter and depth, the average pitting depth, the pitting depth variation coefficient (reflecting the variation in corrosion depth) and the

corrosion density DOP (the ratio of the corroded surface area to the total surface area of the steel plate).

It can be seen that Xia's [11] experimental results tend to be conservative when the average cross-sectional corrosion rate is less than 20%. However, that model ignores the changes in the chemical composition and internal lattice of the steel caused by corrosion, simplifying the factors affecting the tensile strength of the steel and only considering changes in geometric dimensions, which may lead to deviations in the calculated results. Therefore, when establishing a degradation model for the capacity of corroded steel plates with 'average cross-sectional corrosion' as an influencing factor, other factors such as the corrosion density DOP, corrosion location and coefficient of variation (COV) of the pitting depth should also be considered.

4.2. Prediction Model for Yield Strength and Ultimate Strength of Corroded Steel

The relationship between the reduction factor of the yield strength and the average cross-sectional corrosion rate of steel is shown in Figure 8. It can be seen that the reduction factor of the yield strength decreases with the increase in corrosion rate. Through a non-linear fitting regression, a formula for calculating the yield strength reduction factor of corroded steel can be obtained as follows:

$$R_y = 1 - 0.847c^2 - 0.35c \quad (6)$$

where R_y is the reduction factor for the yield strength of the corroded steel, and c is the average corrosion rate.

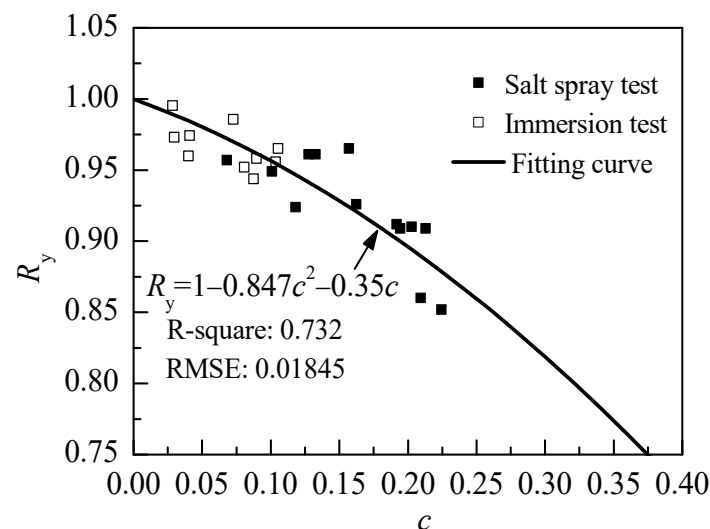


Figure 8. Relationship between reduction coefficient of yield strength and corrosion rate.

The degradation model of the ultimate strength of the corroded steel is similar to that of the yield strength, as shown in Figure 9. It can be observed that the ultimate strength reduction factor of the steel decreases with the increase in corrosion rate. Through non-linear fitting, a formula for calculating the ultimate strength reduction factor of corroded steel can be obtained as follows:

$$R_u = 1 - 1.502c^2 - 0.1c \quad (7)$$

where R_u is the reduction factor for the yield strength of the corroded steel, and c is the average corrosion rate of the steel.

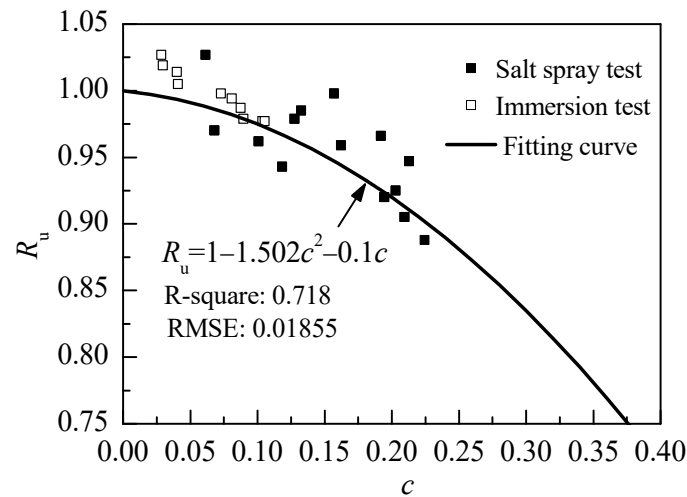


Figure 9. Relationship between ultimate strength reduction factor and corrosion rate.

From Figures 8 and 9, it can be seen that corrosion has a little impact on the yield strength and ultimate strength of the steel. When the average corrosion rate reaches 20%, the yield strength of the steel decreases by approximately 10%, and the ultimate strength decreases by approximately 8%. The influence of corrosion on the yield strength of the steel is slightly greater than that on the ultimate strength, which is consistent with the results of related studies in the literature [5–12].

4.3. Prediction Model for Elastic Modulus of Corroded Steel

Figure 10 shows the relationship between the elastic modulus reduction factor and corrosion rate of corroded steel. The elastic modulus test results are based on the ratio of stress to strain ($\sigma = F/A$, where F is the tensile ultimate capacity of the specimen and A is the cross-sectional area of the specimen). From Figure 10, it can be seen that the elastic modulus linearly decreases with the increase in the corrosion rate of the steel. Through the linear fitting of the experimental data, a degradation model of the reduction factor for the elastic modulus of the corroded steel with the corrosion rate can be obtained as follows.

$$R_E = 1 - 0.344c \quad (8)$$

where R_E is the reduction factor for the elastic modulus of the corroded steel, and c is the average corrosion rate of the steel.

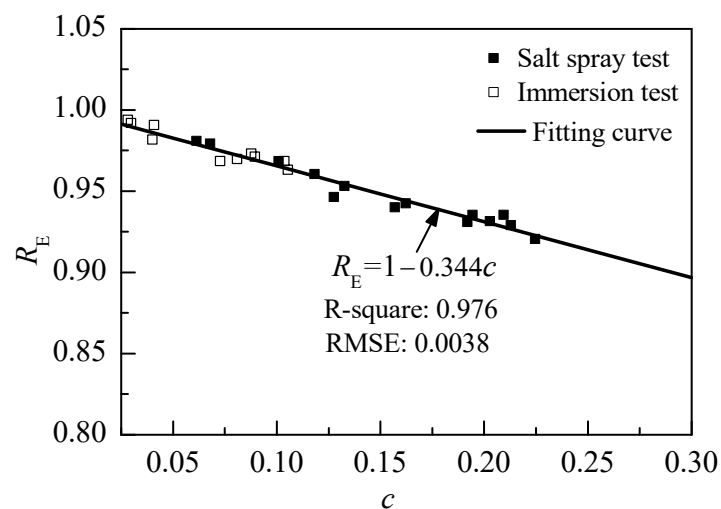


Figure 10. Relationship between elastic modulus reduction factor and corrosion rate.

The maximum deviation between the fitting values and experimental values is 0.97%, with a goodness of fit for the R-squared value = 0.976, indicating a good agreement between the fitting formula and experimental values. The results show that the method of obtaining the elastic modulus by measuring the strain with strain gauges is relatively accurate and stable.

4.4. Prediction Model for Ultimate Strain of Corroded Steel

The ultimate strain of steel can reflect its strengthening ability and ductility. The decrease in the ductility of steel after corrosion is the main reason for brittle failure in steel structures. The determination of the ultimate strain of corroded steel has great significance for establishing the stress–strain relationship of corroded steel. Figure 11 shows the relationship between the reduction coefficient R_ϵ of the ultimate strain of corroded steel and the corrosion rate c . It can be seen from Figure 11 that the ultimate strain ϵ_u shows a significant decreasing trend with the increase in corrosion rate.

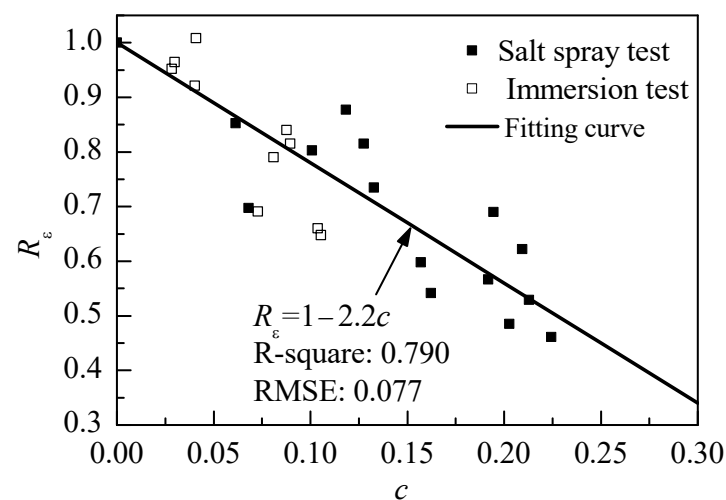


Figure 11. Relationship between ultimate strain reduction factor and corrosion rate.

Through the non-linear fitting of the experimental data, the expression for the ultimate strain reduction factor of the corroded steel is obtained as follows:

$$R_\epsilon = 1 - 2.2c \quad c \leq 0.45 \quad (9)$$

where R_ϵ is the reduction factor for the ultimate strain of the corroded steel, and c is the average corrosion rate of steel.

4.5. Prediction Model for Elongation after Fracture of Corroded Steel

The elongation after fracture is a macroscopic representation of the strain performance of steel, which can reflect the ductility of the steel. Figure 12 shows the relationship between the elongation after fracture and the corrosion rate of the corroded steel. It can be observed from the figure that the percentage elongation after fracture of the corroded steel significantly decreases with the increase in corrosion rate. Through non-linear regression fitting, the degradation model of the percentage elongation after fracture of the corroded steel is developed as follows:

$$R_\delta = 1 - 2.3c \quad c \leq 0.43 \quad (10)$$

where R_δ is the reduction factor for the percentage elongation after fracture of the corroded steel, and c is the average corrosion rate.

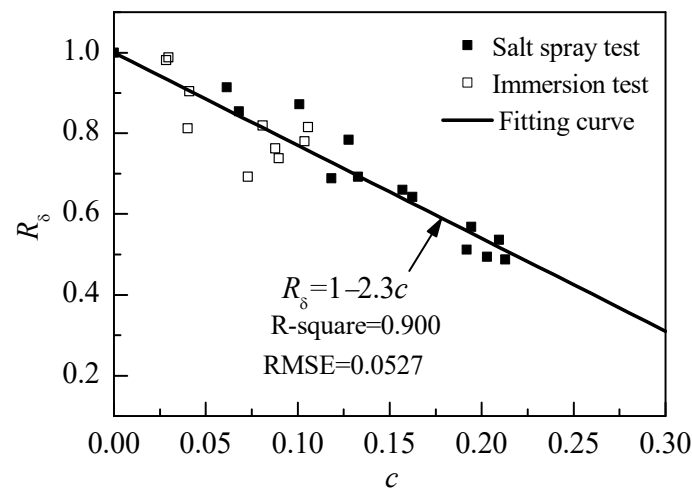


Figure 12. Relationship between reduction factor for percentage elongation after fracture and corrosion rate.

According to the Chinese code GB 50011 [31], the elongation after fracture of structural steel should not be less than 20%. The average percentage of elongation after fracture of the non-corroded steel in this test is approximately 28%. Formula (12) shows that when the corrosion rate of steel is about 12.5%, the percentage elongation after fracture can no longer meet the requirements of the code, indicating that corrosion has had a great impact on the elongation of the steel.

5. Time-Dependent Stress–Strain Curve Model of Corroded Steel

5.1. Evaluation of Prediction Models for Mechanical Properties of Corroded Steel

Currently, a lot of studies have been conducted on the mechanical properties of corroded steel. The main research results based on using the ‘average corrosion’ as the influencing factor are summarized in Table 4. From Table 4, it can be seen that there are different ways to describe the ‘average corrosion’, including the weight loss rate [5–7,11,12] and volume loss rate [9,10]. The concept of ‘average corrosion’ is converting random pitting corrosion into general corrosion, which is a relatively simpler and more practical method. It can directly establish a relationship with the empirical corrosion model, which is currently a trend in development.

Table 4. Evaluation of prediction models for mechanical properties of corroded steel.

Models	R_{σ_y}	R_{σ_u}	R_E	R_δ	c
Tong [5] (2012)	$1 - 0.9852c$	$1 - 0.9732c$	-	$1 - 1.9873c$	Corrosion weight loss rate
Zheng [6] (2015)	$1 - 0.810c$	$1 - 0.707c$	$1 - 0.932c$	$1 - 1.412c$	Corrosion weight loss rate
Zheng [7] (2016)	$1 - 0.9684c$	$1 - 0.438c$	$1 - 0.8913c$	$1 - 1.6459c$	Corrosion weight loss rate
Garbatov [8–10] (2014, 2016, 2022)	$1 - 0.9745c^2 + 0.2362c$	$1 - 0.17c^2 - 0.59c$	$1 - 0.528c$	$1 + 0.6818c^2 - 1.593c$	Corrosion volume loss rate
Xia [11] (2017)	$0.98 - 1.29c$	$0.98 - 1.23c$	-	$0.97 - 45.84c^2 + 1.45c$	Corrosion weight loss rate
Luo [12] (2022)	$1 - 0.7657c$	$1 - 0.7309c$	$1 - 0.8185c$	$1 - 1.9783c$	Corrosion weight loss rate
This research	$1 - 0.847c^2 - 0.35c$	$1 - 1.502c^2 - 0.1c$	$1 - 0.344c$	$1 - 2.3c$	Corrosion weight loss rate

The steel grade used in this research is Q355B, while in the other literature, the steel grade is Q235. The reduction factors for mechanical properties in the model proposed by Garbatov [8–10] eliminate the influence of the steel grade based on the formulas in the literature. The models of Zheng [6,7] are the results of tensile specimens subjected to simulated acidic atmospheric environment and offshore atmospheric environment, respectively.

Compared with other mechanical properties, corrosion has no significant effect on the elastic modulus of the steel. In contrast, the model proposed in this research is closer to the

results of Garbatov's model [8–10]. When the corrosion rate is 30%, the elastic modulus reduction factors of Zheng [6,7], Garbatov [8–10], Luo [12] and this research are 0.736, 0.842, 0.754, and 0.897 respectively, with a maximum deviation of 17.9%. The reason why it is difficult to accurately obtain the elastic modulus of corroded steel in experiments is that the elastic modulus is obtained by the ratio of stress to strain. However, the calculation of stress involves many influencing factors ($\sigma = F/A_r$, the cross-sectional area of corroded steel is usually calculated by the weight loss method, and there may be some deviation in the process of rust removal and weighing). In the test, the elastic modulus of steel in the elastic stage is not an 'absolutely constant value', and there are differences in the method for determining this value.

As for the yield strength and ultimate strength of corroded steel, the prediction models proposed by researchers are different due to the randomness of pitting pits, including natural pitting and mechanical pitting. The strength reduction formula proposed in this research is closer to the results of Garbatov's model [8–10], while the formulas proposed by other researchers are more conservative. When the corrosion rate is less than 30%, the maximum deviation between the calculated results of the formula and Soares's results is 4.8%.

The analysis of the influence of corrosion on the mechanical properties of materials revealed that the most severely deteriorated mechanical properties indicator of steel after corrosion is the percentage of elongation after fracture. Thus, the limit value for the corrosion rate of steel is controlled by the percentage of elongation after fracture. Comparisons of models between the reduction factor of elongation after fracture and the corrosion rate are shown in Figure 13. It can be seen that the results predicted by Garbatov [8–10] and Zheng [6,7] are closer. The result in this research is closer to the models proposed by Tong [5] and Luo [12].

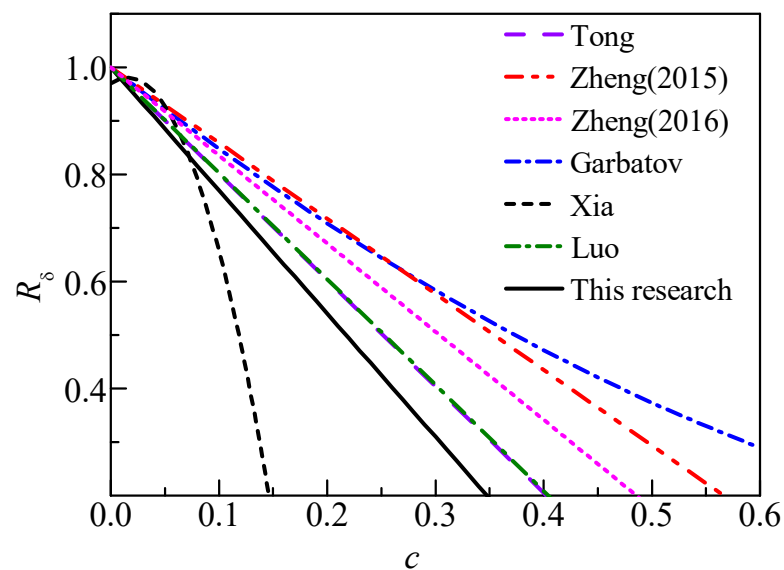


Figure 13. The comparisons of models between reduction factor of percentage elongation after fracture and corrosion rate [5–12].

Based on the requirements of the specifications for elongation [31], the percentage elongation after fracture of structural steel should not be less than 20%. Combined with current research results [5–10,12], a formula for calculating the allowable corrosion rate of steel is developed as follows:

$$[c] = -0.7\delta_0^2 + 5.4\delta_0 - 0.8 \quad \delta_0 \leq 0.386 \quad (11)$$

where $[c]$ is the maximum allowable corrosion rate of the steel. δ_0 is the initial percentage of elongation after fracture of the steel.

The elongation can represent the extent of residual deformation and the ability of steel to undergo plastic deformation, ensuring that structural members have a sufficient plastic deformation capacity during earthquakes. According to Equation (11) and Figure 14, it can be seen that the maximum allowable corrosion rate of the steel is closely related to the initial elongation. For example, when the initial elongation is 30%, the maximum allowable corrosion rate is 19.2%. The maximum allowable corrosion rate formula provides a scientific basis for the regular maintenance of structures, preventing brittle damage or even the collapse of structures due to corrosion.

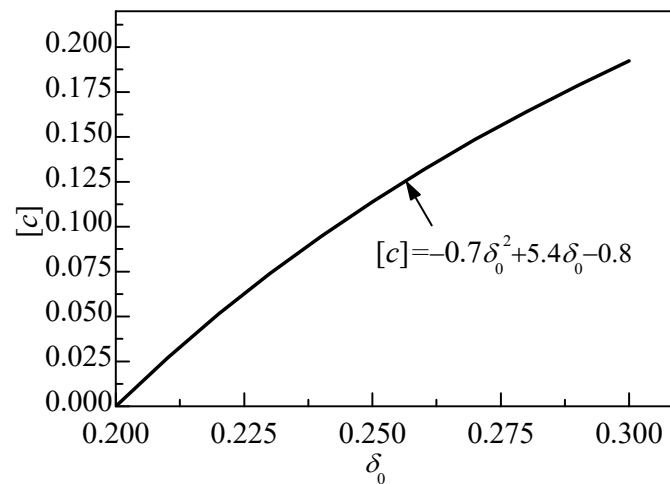


Figure 14. The maximum allowable corrosion rate of the steel.

5.2. Establish Time-Dependent Stress–Strain Curve Model of Corroded Steel

The tensile testing process of low-alloy steel includes an elastic stage, elastic–plastic stage, plastic stage and strengthening stage. The stress–strain curves of the non-corroded steel and corroded steel are shown in Figures 15a and 15b, respectively.

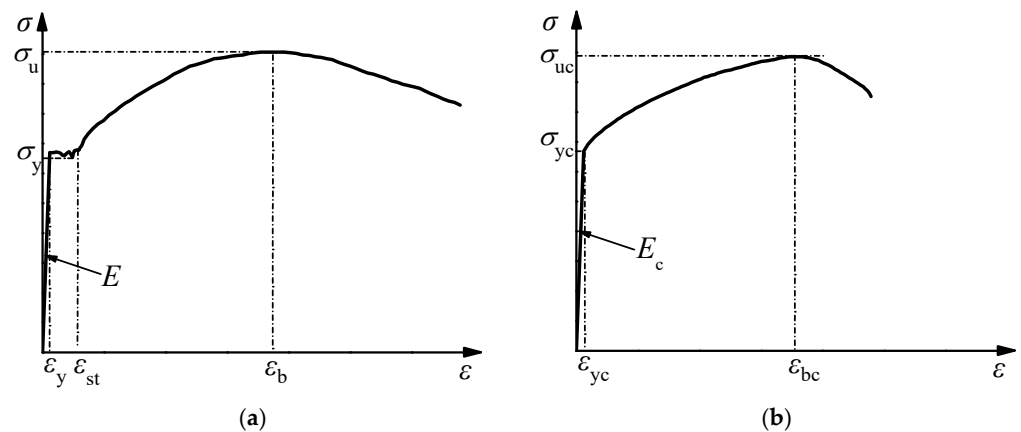


Figure 15. Stress–strain curve of low-alloy steel. (a) Stress–strain curve of non-corroded steel; (b) stress–strain curve of corroded steel.

The experimental results of this study indicate that, in addition to the decrease in yield strength, ultimate strength and elastic modulus after corrosion, the most significant change in the stress–strain curve of the corroded steel is the noticeable shortening or even disappearance of the yield platform, as well as the degradation and shortening of the elastic–plastic stage and strengthening stage. With the increase in the corrosion rate, the length of the yield platform of the steel gradually shortens, that is, $\epsilon_{st} \rightarrow \epsilon_y$ (ϵ_{yc}). According to the tensile test stress–strain curve results, when the corrosion rate $c = 0\%$ and $\epsilon_{st} = 0.02$, the steel yield platform was obvious. However, when c is about 13% and $\epsilon_{st} = 0.015$ (specimen F3),

and when $c > 13\%$ and $\varepsilon_{st} = \varepsilon_{yc}$, the yield platform of corroded steel is no longer obvious, and the value at the end of the yield platform equals that at the beginning.

The accurate inputs for the constitutive model of the corroded steel are crucial for the non-linear buckling analysis, ultimate capacity calculations and large deformation analysis of the corroded structural members. Based on the experimental results in this research, the stress–strain relationship model of the corroded steel can be established as shown in the following formula:

$$\left. \begin{aligned} \sigma_{yc} &= (1 - 0.847c^2 - 0.35c)\sigma_y \\ \sigma_{uc} &= (1 - 1.502c^2 - 0.1c)\sigma_u \\ E_c &= (1 - 0.344c)E \\ \varepsilon_{bc} &= (1 - 2.2c)\varepsilon_b \\ \varepsilon_{yc} &= \frac{\sigma_{yc}}{E_c} \\ \varepsilon_{st} &= \varepsilon_{yc} \quad c \geq 0.13 \\ c &= \frac{d(T)}{t_0} \end{aligned} \right\} \quad (12)$$

where σ_y is the yield strength of the non-corroded steel. σ_{yc} is the yield strength of the corroded steel. σ_u is the ultimate strength of the non-corroded steel. σ_{uc} is the ultimate strength of the corroded steel. E is the elastic modulus of the non-corroded steel. E_c is the elastic modulus of the corroded steel. ε_y is the elastic strain of steel (the starting point strain of the yield platform). ε_{st} is the elastoplastic strain of the steel (the end strain of the yield platform). ε_{yc} is the elastic strain of the corroded steel. ε_b is the strain of the corroded steel. ε_{bc} is the ultimate strain of the corroded steel. $d(T)$ is the average corrosion depth of the steel. t_0 is the initial thickness of the steel. c is the average corrosion rate, which is related to the corrosion environment, applied stress and corrosion time.

Therefore, it is necessary to determine the mechanical property model of the corroded steel according to the natural corrosion environment and exposure time of the steel structure. Based on the relationship model established in this research between the mechanical properties of the corroded steel and the average corrosion rate, a predictive model can be further derived to describe the time-dependence of the steel's mechanical properties, considering the coupling effect of the corrosion environment and external stress.

For example, according to the corrosion data of carbon steel exposed to typical marine atmospheric environments (Qingdao, China) and industrial atmospheric environments (Jiangjin, China), as well as the model for calculating the acceleration corrosion in steel due to elastic stress in the research [32], an average corrosion rate model that simultaneously considers the corrosion environment, external stress and corrosion time can be established. The average corrosion rate of steel considering the applied stress in a typical marine atmospheric environment (Qingdao area, China) is as follows:

$$c = \frac{0.0695T^{0.578}\alpha}{t_0} \quad (13)$$

In a typical marine atmospheric environment (Jiangjin, China), the average corrosion rate of steel considering external stress is as follows:

$$c = \frac{0.0802T^{0.415}\alpha}{t_0} \quad (14)$$

where T is the atmospheric corrosion exposure time, in years (a), and α is the stress corrosion acceleration factor. For carbon steel and low-alloy steel, $\alpha = \exp(1.94 \times 10^{-3}\sigma)$ [32]. t_0 is the initial thickness of steel.

The stress–strain curve of the corroded steel established in this research considers the combined influences of corrosion environment, applied stress and corrosion time on the mechanical properties of the steel. Based on the actual corrosion environment and stress information, the dynamic variation in the mechanical properties of the steel with the corrosion time can be obtained. The research results can provide a basis for predicting

the life of steel in a corrosive environment and can also provide a reference for defining a material constitutive model in a non-linear finite element analysis of corroded steel structural members.

6. Verification of Time-Dependent Stress–Strain Curve Model of Corroded Steel

6.1. Test Stud Columns

The experimental program includes six cold-formed square stud columns, of which two are non-corroded columns, and four are corroded columns [33]. The stud columns were subjected to the salt spray and alternate immersion test, with the same corrosion conditions as the material test specimens, as shown in Table 2. The corroded columns of 1800 h and 3600 h under the salt spray condition and 480 h and 960 h under the alternate immersion condition were obtained. The geometric dimensions of the columns before and after corrosion are detailed in Table 5 [34,35].

Table 5. Dimensions of square stud columns.

Specimens	Corrosion Method	Corrosion Time (h)	t_w (mm)	t_f (mm)	t_c (mm)	c (%)	A_0 (mm ²)	A_r (mm ²)	L (mm)
R300-0-1	-	-	3.87	3.86	0	0	1490.3	1490.3	300.0
R300-0-2			3.89	3.92	0	0	1508.0	1508.0	299.7
R300-F-1	Salt spray test	1800	3.43	3.46	0.521	13.02	1514.9	1332.6	299.7
R300-F-2		3600	3.92	3.91	0.824	20.61	1507.1	1159.3	299.1
R300-I-1	Alternate immersion test	480	3.63	3.59	0.308	7.69	1506.0	1395.1	299.5
R300-I-2		960	3.50	3.53	0.418	10.46	1507.3	1362.4	298.8

For R300-X–Y, R300 specimens are square with length of 300 mm; X is ‘0’, indicating a non-corroded parallel specimen; X is ‘F’ for salt spray test specimen; X is ‘I’ for alternate immersion test specimen; and Y represents ‘1’ or ‘2’. For non-corroded specimens, it indicates two parallel specimens; for corroded specimens, it represents different corrosion times.

6.2. Test Process

The axial compression test was conducted through a 2000 kN electro-hydraulic testing machine, as shown in Figure 16. Due to the spherical joint of the upper loading plate of the testing machine, a fixed frame was designed to secure the spherical joint support to prevent rotation during loading. A TST3827E static–dynamic data acquisition instrument was used for data collection. Prior to formal loading, the center point of the column was aligned with the axis on the press base, and a 60 kN force was applied to preload the column. After the adjustment work was completed, the force was unloaded to a relatively small value (set to 5 kN in this test) to eliminate possible gaps between the ends of the column and the press base. The test loading was carried out using a force-displacement comprehensive control method, which can be set through the program control mechanism of the pressure testing machine software. First of all, a constant rate force control was adopted with a loading speed of 0.5 kN/s, a load step of 50 kN and a holding time of 60 s for each load step [34]. When the load reaches 80% of the estimated ultimate capacity, it switches to the displacement control. The constant rate displacement control was set to 0.1 mm/min (maintained for two steps, then changed to 0.2 mm/min), with a displacement control of 0.2 mm for each step. The displacement holding time of each stage was set to 60 s. After reaching the peak load, the loading continued until it dropped to 80% of the peak load, at which point the loading stopped.

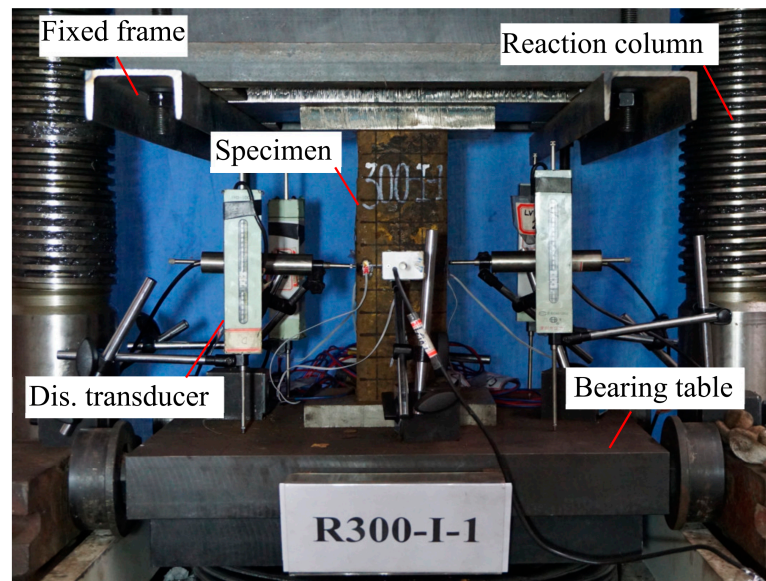


Figure 16. Test setup.

6.3. Test Results

The non-corroded and accelerated corroded square stub columns all experienced strength failure, and the failure modes of the columns are shown in Figure 17. The stub column failure occurred where the local imperfection was largest. The failure mode was characterized by a local buckling along the width and height directions of the column section, forming a single wave, with a wavelength almost equal to the height of the column section. Before reaching the ultimate capacity, there was no visible buckling failure phenomenon inside the column. When the column approached the ultimate load, the local buckling occurred and then the column failed.

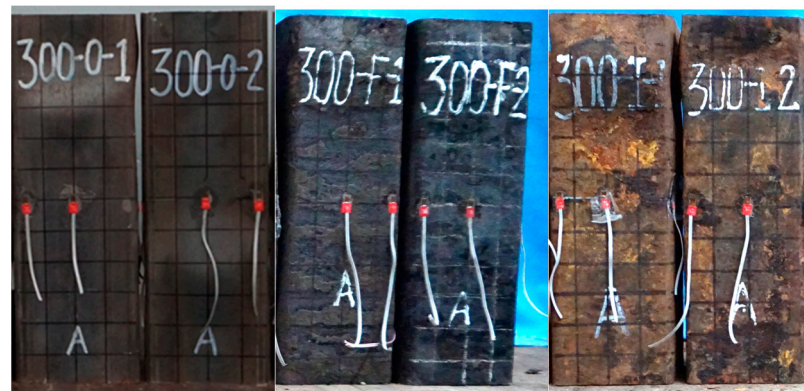


Figure 17. Failure modes of stub columns.

A comparison between the test ultimate capacity F and calculation capacity F^* in Equation (12) is shown in Table 6. In Table 6, $\sigma_{uc} = (1 - 1.502c^2 - 0.1c)\sigma_u$ and $F^* = \sigma_{uc}A_r$. It can be seen that due to the developed formula not considering the influence of residual stresses and initial geometric imperfections, the formula results for the non-corroded columns are 4.75% higher than the experimental results (for R300-01, it is 4.8%, and for R300-0-2, it is 4.7%). For the corroded columns, the maximum deviation between the formula result and the experimental result is 13.6%. If we subtract the deviation caused by residual stress and initial geometric imperfections, it indicates that the maximum deviation in predicting the remaining capacity of the corroded columns by the formula developed in this research study is within 8.5%. This demonstrates that the developed formula for the

degradation of the mechanical properties of corroded steel has a good level of accuracy and can be used for predicting the remaining capacity of corroded members.

Table 6. Ultimate capacity of stub columns.

Specimens	A_r (mm ²)	c (%)	Failure Mode	F (kN)	σ_{uc} (MPa)	F^* (kN)	F/F^*
R300-0-1	1490.3	0	SF	736.6	519.2	773.8	0.952
R300-0-2	1508.0	0	SF	746.3	519.2	783.0	0.953
R300-F-1	1332.6	13.02	SF	583.4	499.2	665.3	0.877
R300-F-2	1159.3	20.61	SF	482.8	475.4	551.1	0.876
R300-I-1	1395.1	7.69	SF	651.6	510.6	712.3	0.915
R300-I-2	1362.4	10.46	SF	594.7	505.2	688.3	0.864

SF represents the strength failure of column.

7. Conclusions and Further Work

In order to study the degradation laws of the mechanical properties of corroded Q355B structural steel, a salt spray test and an immersion test were carried out to obtain corroded specimens with different corrosion rates. Then, tensile tests were conducted to study the influence of corrosion on the mechanical properties of steel. A simplified time-dependent stress–strain model of the Q355B structural steel was developed and verified by axial compression testing of the stud columns. The following conclusions were drawn:

- (1) There are some differences in the micro-morphology of corroded steel subjected to a simulated marine atmosphere and an industrial atmosphere. Compared with the marine atmosphere specimens, the industrial atmosphere specimens' cracks developed rapidly, and the surfaces of the specimens were porous, soft and accompanied by delamination. The industrial atmospheric specimens developed cracks more rapidly compared to the marine atmospheric specimens, with lower levels of surface roughness, soft rust layers and a stratified appearance.
- (2) Corrosion not only deteriorates strength characteristics, but also significantly reduces deformability, leading to brittle failure. With the increase in corrosion rate, the stress–strain curve of steel undergoes significant changes, mainly manifested as a significant decrease in the ultimate strain and the shortening or even disappearance of the yield platform. When the corrosion rate is greater than 13%, the yield platform is no longer obvious and should not be considered.
- (3) The elongation after fracture is the most severely deteriorated mechanical property of corroded steel (even below 10%). Based on the experiment and current research results, the maximum allowable corrosion rate of the steel is established as $[c] = -0.7\delta_0^2 + 5.4\delta_0 - 0.8$, which can serve as the basis for the regular maintenance of structures, avoiding brittle damage or even accidents involving collapses.
- (4) A simplified time-dependent stress–strain model of Q355B structural steel is established considering the coupling effects of corrosive environments and applied stress. An axial compression test was conducted for the effectiveness of the established model. It shows that the model has a maximum prediction deviation of within 8.5% for the assessment of the remaining capacity of the columns. The stress–strain model can be used for finite element analyses of aged structures and fitness-for-purpose analyses in structural integrity assessments.

In the present study, a 4 mm thick corroded Q355B structural steel was analyzed. The relationships for other thicknesses need to be studied in the future, since thicker plates are often used in steel structures. This research establishes a time-dependent stress–strain curve model for corroded steel and verifies it through axial compression tests on stud columns. The evaluation of the rationality of the established model is insufficient and should provide a basis for further studies. Experimental studies will be carried out on the bending, shear and flexural–torsional buckling behavior of corroded members. Furthermore, finite element models need to be established to verify the effectiveness of the proposed model.

Author Contributions: Conceptualization, Y.C.; Data curation, Y.C.; Formal analysis, Y.C. and B.M.; Investigation, B.M.; Methodology, Y.C. and R.L.; Software, Y.C.; Supervision, R.L.; Validation, Y.C. and R.L.; Visualization, Y.C.; Writing—original draft, Y.C.; Writing—review and editing, Y.C. All authors have read and agreed to the published version of the manuscript.

Funding: This research was supported as part of a Doctor of Entrepreneurship and Innovation in Jiangsu Province (Grant No. JSSCBS20221257) and Jiangsu University of Science and Technology Youth Science and Technology Innovation Project (Grant No. 2021TJ170J).

Data Availability Statement: The data presented in this study are available from the corresponding author upon request. The data are not publicly available due to the policies of the data provider.

Conflicts of Interest: The authors declare no conflicts of interest.

References

1. Paik, J.K.; Lee, J.M.; Ko, M.J. Ultimate compressive strength of plate elements with pit corrosion wastage. *Proc. Inst. Mech. Eng. M-J. Eng.* **2003**, *217*, 185–200. [[CrossRef](#)]
2. Nakai, T.; Matsushita, H.; Yamamoto, N. Effect of pitting corrosion on local strength of hold frames of bulk carriers (1st report). *Mar. Struct.* **2004**, *17*, 403–432. [[CrossRef](#)]
3. Ahmmad, M.M.; Sumi, Y. Strength and deformability of corroded steel plates under quasi-static tensile load. *J. Mar. Sci. Technol.* **2010**, *15*, 1–15. [[CrossRef](#)]
4. Appuhamy, J.; Kaita, T.; Ohga, M.; Fujii, K. Prediction of Residual Strength of Corroded Tensile Steel Plates. *Int. J. Steel Struct.* **2011**, *11*, 65–79. [[CrossRef](#)]
5. Shi, W.Z.; Tong, L.W.; Chen, Y.Y. Experimental study on influence of corrosion on behavior of steel material and steel beams. *J. Build. Struct.* **2012**, *33*, 53–60. (In Chinese)
6. Zheng, S.S.; Wang, X.F.; Han, Y.Z.; Tian, J.; Cheng, Y.; Sun, L.B. Experimental study on seismic behavior of multi-aged steel frame columns in acidic atmospheric environment. *China Civil Eng. J.* **2015**, *48*, 47–59. (In Chinese)
7. Zheng, S.S.; Zhang, X.H.; Wang, X.F.; Cheng, Y.; Sun, L.B. Experimental research on seismic behaviors of multi-aged steel frame columns in the offshore atmospheric environment. *China Civil Eng. J.* **2016**, *49*, 69–77. (In Chinese)
8. Garbatov, Y.; Soares, C.G.; Parunov, J.; Kodvanj, J. Tensile strength assessment of corroded small scale specimens. *Corros. Sci.* **2014**, *85*, 296–303. [[CrossRef](#)]
9. Garbatov, Y.; Parunov, J.; Kodvanj, J.; Soares, C.G. Experimental assessment of tensile strength of corroded steel specimens subjected to sandblast and sandpaper cleaning. *Mar. Struct.* **2016**, *49*, 18–30. [[CrossRef](#)]
10. Woloszyk, K.; Garbatov, Y.; Kłosowski, P. Stress-strain model of lower corrode steel plates of normal strength for fitness-for-purpose analyses. *Constr. Build. Mater.* **2022**, *323*, 126560. [[CrossRef](#)]
11. Sheng, J.; Xia, J.W. Effect of simulated pitting corrosion on the tensile properties of steel. *Constr. Build. Mater.* **2017**, *131*, 90–100. [[CrossRef](#)]
12. Luo, L.S.; Fu, H.L.; Zhang, Y.Q.; Xie, X.R. Experimental Study on the Overall Stability of Corroded H-Shaped Steel Beams. *Buildings* **2022**, *12*, 1923. [[CrossRef](#)]
13. Wang, R.H. On the effect of pit shape on pitted plates, Part II: Compressive behavior due to random pitting corrosion. *Ocean Eng.* **2021**, *236*, 108737. [[CrossRef](#)]
14. Xu, S.H.; Zhang, H.J.; Wang, Y.D. Estimation of the properties of corroded steel plates exposed to salt-spray atmosphere. *Corros. Eng. Sci. Technol.* **2019**, *54*, 431–443. [[CrossRef](#)]
15. Xu, S.H.; Zhang, Z.X.; Li, R.; Wang, H. Effect of cleaned corrosion surface topography on mechanical properties of cold-formed thin-walled steel. *Constr. Build. Mater.* **2019**, *222*, 1–14. [[CrossRef](#)]
16. Zhao, N.; Zhang, C.T. Experimental Investigation of the Mechanical Behavior of Corroded Q345 and Q420 Structural Steels. *Buildings* **2023**, *13*, 475. [[CrossRef](#)]
17. Jia, C.; Shao, Y.; Guo, L.; Liu, Y. Mechanical properties of corroded high strength low alloy steel plate. *J. Constr. Steel Res.* **2020**, *172*, 106160. [[CrossRef](#)]
18. Wu, H.Y.; Lei, H.G.; Chen, Y.F. Grey relational analysis of static tensile properties of structural steel subjected to urban industrial atmospheric corrosion and accelerated corrosion. *Constr. Build. Mater.* **2022**, *315*, 125706. [[CrossRef](#)]
19. Soares, C.G.; Garbatov, Y. Reliability of maintained, corrosion protected plates subjected to non-linear corrosion and compressive loads. *Mar. Struct.* **1999**, *12*, 425–445. [[CrossRef](#)]
20. Standardization Administration of the People's Republic of China. *Steel and Steel Products-Location and Preparation of Samples and Test Pieces for Mechanical Testing*; China Standards Press: Beijing, China, 2018.
21. Standardization Administration of the People's Republic of China. *Metallic Materials-Tensile Testing-Part 1: Method of Test at Room Temperature*; China Standards Press: Beijing, China, 2021.
22. Standardization Administration of the People's Republic of China. *High Strength Low Alloy Structural Steels*; China Standards Press: Beijing, China, 2018.

23. State Administration for Market Regulation and Standardization Administration of the People's Republic of China. *Corrosion Tests in Artificial Atmospheres—Salt Spray Tests*; China Standards Press: Beijing, China, 2021. (In Chinese)
24. ASTM. *Standard Practice for Modified Salt Spray (Fog) Testing Annual Book of ASTM Standards*; ASTM Special Technical Publication: West Conshohocken, PA, USA, 2011.
25. Ministry of Railways of the People's Republic of China. *Test Method for Periodic Wetted Corrosion of Weathering Steels for Railway Use*; China Standards Press: Beijing, China, 2003. (In Chinese)
26. General Administration of Quality Supervision, Inspection and Quarantine of the People's Republic of China. *Corrosion of Metals and Alloys-Alternate Immersion Test in Salt Solution*; China Standards Press: Beijing, China, 2018. (In Chinese)
27. Tian, Y.W.; Chen, X.Q.; Li, X.G. A study of simulated indoor accelerated testing method for marine atmospheric correlation. *Corros. Prot.* **2014**, *35*, 781–784. (In Chinese)
28. Qiu, B. The Study on Surface Characteristics and Eccentric Compressive Load-Capacity of Corroded H-Shape Steel Members at Neutral Salt Fog Environment. Ph.D. Dissertation, Xi'an University of Architecture and Technology, Xi'an, China, 2014. (In Chinese)
29. Shu, G.P.; Chen, Y.; Lu, R.H.; Wu, C.F. Corrosion behavior of structural steel in simulated marine and industrial atmosphere environment. *J. Xi'an Univ. Arch. Tech. Nat. Sci. Ed.* **2022**, *54*, 475–478+490. (In Chinese)
30. The Standards Policy and Strategy Committee. *Corrosion of Metals and Alloys-Removal of Corrosion Products from Corrosion Test Specimens*; International Organization for Standardization: Geneva, Switzerland, 2014.
31. Ministry of Housing and Urban-Rural Development of the People's Republic of China. *Code for Seismic Design of Building*; China Architecture & Building Press: Beijing, China, 2016. (In Chinese)
32. Chen, Y. Research on the Degradation of Steel Structures for the Needs of Structural Life-Cycle Design and Time-Dependent Reliability in Corrosive Environment. Ph.D. Dissertation, Southeast University, Nanjing, China, 2021. (In Chinese)
33. American Institute of Steel Construction Committee. *Specification for Structural Steel Buildings*; AISC: Chicago, IL, USA, 2016.
34. Chen, Y.; Shu, G.P.; Zheng, B.F.; Lu, Y.H. Local buckling behaviour of welded π -shaped compression stub columns. *J. Constr. Steel Res.* **2019**, *154*, 224–234. [[CrossRef](#)]
35. Ziemian, R.D. *Guide to Stability Design Criteria for Metal Structures*, 6th ed.; John Wiley & Sons, Inc.: New York, NY, USA, 2010; pp. 12–62.

Disclaimer/Publisher's Note: The statements, opinions and data contained in all publications are solely those of the individual author(s) and contributor(s) and not of MDPI and/or the editor(s). MDPI and/or the editor(s) disclaim responsibility for any injury to people or property resulting from any ideas, methods, instructions or products referred to in the content.